

# Simulation of Anisotropic Crystalline Etching using a Continuous Cellular Automata Algorithm

Zhenjun Zhu, Chang Liu<sup>1</sup>

**Abstract:** We present results on the development of an anisotropic crystalline etching simulation (ACES) program based on a new continuous Cellular Automata (CA) model, which provides improved spatial resolution and accuracy compared with the conventional and the stochastic CA methods. Implementation of a dynamic CA technique provides increased simulation speed and reduced memory requirement (5x). A first ACES software based on common personal computer platforms has been realized. Simulated results of etching match well with experiments. We have developed a new methodology to obtain the etch-rate diagram of anisotropic etching efficiently using both experimental and numerical techniques.

**keyword:** etching simulation, anisotropic etching, cellular automata, continuous cellular automata

## 1 Introduction

### 1.1 Anisotropic etching

Anisotropic etching [Bean (1978)] of silicon is a prevalent technique for realizing 3D MEMS structures [Madou (1997), Petersen (1982)]. The process has been used for many applications, including sensors (e.g., cavities of pressure sensors [Petersen (1982)] and probes of scanning probe microscopes [Liu and Gamble (1998)]), communications (e.g., micromachined antennas [Ling and Rebeiz (1992)]), and biomedical engineering (neuron wells [Wright, Tatic-Lucic, Tai, Maher, Dvorak and Pine (1996)]), to name only a few. The etching can be accomplished using several chemical etching systems, including ethylene-diamine pyrocatechol (EDP) and potassium hydroxide (KOH). Three-dimensional profiles resulting after timed etch are determined both by the 3D etch rate distribution and by initial conditions, including mask patterns and the initial 3D profile of the substrate. As MEMS design and fabrication become increasingly sophisticated, efficient and accurate anisotropic etching simulation becomes more important.

### 1.2 Etching simulation

Models for simulating the etching process fall into two categories: the geometric models and cellular automata (CA) models.

#### 1.2.1 Geometrical model

In a geometric model, the resultant 3D shape after an elapsed period of etching is determined by geometric rules [Sequin (1991), Frank and Ives (1960), Hubbard and Antonsson (1994), Heim (1993)]. The Wulff-Jacodine model [Jaccodine (1962), Shaw (1979), Danel and Delapierre (1992), Buser and de Rooij (1991)], for example, uses plane waves that propagate at a rate determined by the etch-rate diagram. To our knowledge, several simulators [Li, Hubbard and Antonsson (1998), Asaumi, Iriye and Sato (1997)] based on geometric models have been reported. The semiconductor substrate is treated as a continuous entity. A 3D continuous geometric description, or mesh, can be used easily in visualization or post-process. One major disadvantage of geometric models lies in the fact that it does not efficiently process complex structures with merging features.

#### 1.2.2 Cellular automata (CA) model

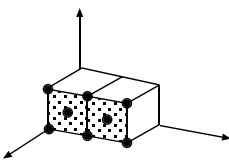
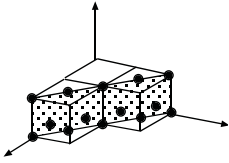
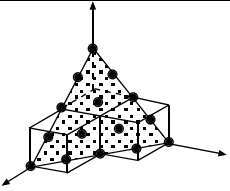
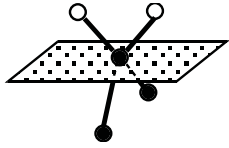
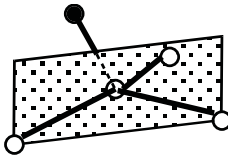
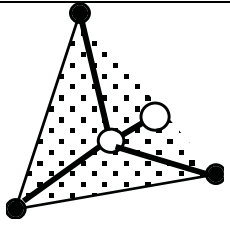
In contrast to the geometric model, the CA model exhibits high efficiency and accuracy when handling arbitrarily complex mask shapes and merging of 3D structures. In the CA method [Than and Buttgenbach (1994)] a substrate is represented by a 3D array of discrete cells that reside in a crystalline lattice (Fig. 1). Etching of the substrate material, represented by discrete spatial, temporal, and cell-state variables, is represented by removal of individual atoms according to etching rules. During etching, the decision to remove or retain a particular cell will be based on the link status of its lattice neighbors according to cell-removal rules. The link status (Tab. 1) is categorized by the number of neighboring cells and their relative positions; each case corresponds to the magnitude of chemical bonds. Several reported simulation programs (e.g., AnisE [Marchetti, He, Than and Akkaraju (1998)], ASECA [Nishidate, Baba and Gaylord (1998)] and SUZANA [Buttgenbach and Than (1996)]) have been implemented based on the CA method.

We have focused on a CA-based method due to its ability to handle complex geometry. A new CA method, called the continuous CA method, has been developed to realize higher accuracy in the simulation. This method will be reviewed in Sec. 2 after discussing the constraints of conventional and stochastic CA methods in the next two sections.

---

<sup>1</sup> Micro Actuators, Sensors and Systems Group, 208 North Wright Street, University of Illinois, Urbana, IL 61801.

**Table 1** : Conventional CA rules

Surface	{100} surface	{110} surface	{111} surface
Schematic diagram			
Neighbor status of a atom on the surface			
Etched neighbor number	2	1	1
Untouched neighbor number	2	1	3
Neighbor on the surface	0	2	0
Result in traditional CA model	Remove	Remove	Keep

### 1.2.3 The stochastic CA model

The demand for high accuracy and efficiency in MEMS CAD tools is increasing [Senturia, Aluru and White (1997), Karam and Courtois (1996)]. Conventional CA modeling utilizes discrete cell states; that is, a cell within a lattice can only assert one of two states: “removed” or “retained”. Consequently, normalized etch rates along major crystal axes can have two possible values: 1 (indicating finite etch rate) or 0 (indicating zero etch rate). It is noticeable from Tab. 1 that the conventional CA method only allows discrete etch-rate ratios along certain directions of the semiconductor crystal (e.g., major crystal axes including  $\langle 100 \rangle$ ,  $\langle 110 \rangle$ , and  $\langle 111 \rangle$ ). The default ratio of etch rates (for silicon) in three major axes,  $\langle 100 \rangle$ ,  $\langle 110 \rangle$ , and  $\langle 111 \rangle$ , equals  $1:\sqrt{2}:0$ . Obviously, this model oversimplifies the physical etching process. For example, the etch rate of  $\{111\}$  surfaces, though small, is not completely zero; according to [Petersen (1992)], anisotropic etch rate ratios among  $\langle 100 \rangle$  and  $\langle 111 \rangle$  directions are equal to 35 and 400 for EDP and KOH (30 wt%), respectively. In addition, the ratio of etch rates for  $\{100\}$  and  $\{110\}$  surfaces are not constant.

In order to accommodate physically realistic etch rate ratios encountered, the conventional CA method must be modified. In a stochastic CA algorithm [Than and Buttgenbach (1994)], the probability of a cell being removed during a particular etch step is not only determined by the neighbor link status (ac-

ording to rules in Tab. 1), but also by an assigned random number  $P_e$ . At every etch step and for each cell, the value of assigned  $P_e$  will be compared with a prescribed threshold value  $P_t$ , which corresponds to the relative etch rate in a particular lattice axis. If  $P_e$  is greater than  $P_t$ , a cell will be removed; if not, it will be retained within the lattice. For example, if the etch rate of  $\{110\}$  planes is 0.5 (normalized against the etch rate of fastest-etching  $\{100\}$  planes),  $P_t$  is set to 0.5. Statistically, only half the cells on an exposed  $\{110\}$  surface will be removed at each step.

The stochastic CA model can handle arbitrary etch-rate ratios among major axes. However, it will result in roughened surfaces due to randomized cell removal from an atomically smooth crystal plane. The roughness, regarded as noise in simulation results, is within 1 atom constant of the lattice, reduces the accuracy of simulation. This results in difficulties of defining edges and planes, and visual rendering of simulation results.

## 2 Continuous CA model

The new continuous CA method, compared with the stochastic CA model, allows arbitrary etch-rate ratios among major axes but avoids generating artificially roughened surfaces and therefore causes no loss of resolution and accuracy. As a fundamental difference between this and other existing CA models (conventional or stochastic), each cell in the system can

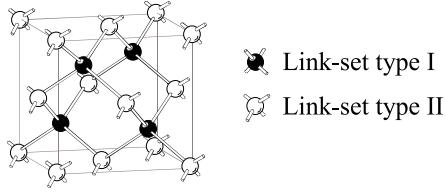


**Figure 1** : Schematic diagram of a diamond crystal lattice

have nondiscrete state variables, with their values ranging continuously between 0 and 1. One convenient nondiscrete state of a cell is its mass (denoted  $M$ ). A cell can assume arbitrary states between  $M = 0$  (“removed”) and  $M = 1$  (“un-etched”), corresponding to its extent of removal.

Arbitrary etch rates are incorporated using this new nondiscrete state designation. During every etch step (with an associated time  $T$ ), the mass of a cell (ranging between 0 and 1) will be reduced by an amount that corresponds to the etch rate of the surface on which the cell resides. As an example, if the etch rate of  $\{110\}$  planes is 0.5 cells per step (normalized with respect to the fastest etch rate among all major low-index planes), the mass of cells on these surfaces will decrease by 0.5 in each step. If a cell is previously un-etched (i.e.,  $M = 1$ ), for example, the value of  $M$  would be reduced to 0.5 in one etch step. Should the etch process continue, the mass will subsequently be reduced to 0% during the next step. The corresponding etch rate is therefore 0.5 cells per step.

Rules for continuous cell-removing under arbitrary etch rate ratios have been developed. Assuming that the desired etch rate on a particular crystal plane is  $E_s \in [0, 1]$ , and the elapsed time of each etch step is  $T$  (with the default value being 1), then the number of etch steps ( $N_T$ ) that are required to completely remove a cell equals<sup>2</sup>

$$N_T = \left\lceil \frac{M}{E_s T} \right\rceil. \quad (1)$$

If  $M$  is an exact multiple of  $E_s T$ , the effective etch rate of a surface, denoted  $E'_s$ , is equal to the desired etch rate:

$$E'_s = \frac{M}{N_T T} = \frac{M}{\left(\frac{M}{E_s T}\right) T} = E_s. \quad (2)$$

On the other hand, difficulties could arise if  $M$  is not a multiple of  $E_s T$ . In such cases, the value of the effective etch rate would differ from that of the target etch rate, namely,

$$E'_s = \frac{M}{\left\lceil \frac{M}{E_s T} \right\rceil T} \neq E_s. \quad (3)$$

Under these common circumstances, independent removal of a single cell is not possible because the mass of at least one

<sup>2</sup>  $A = \lceil B \rceil$  means that  $A$  is the smallest integer that is greater than  $B$ .

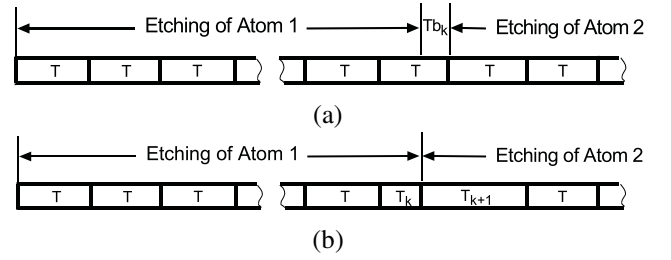


**Figure 2** : Simulation process (a) without time compensation and (b) with time compensation.

neighboring cell must be simultaneously adjusted during the last step ( $N_T$ ) of the cell removal. However, a cell-removal algorithm that involves multiple cells is not desirable because the memory must be increased to accommodate idle cells. A cell-removal rule based on concurrent, active cells at the interface of the silicon material and the etching solutions is desirable. In order to achieve this goal, a time compensation method is introduced; it is explained in the following paragraph.

When a cell is removed during an etch-step  $k$ , the etching of the next cell will not begin immediately until the next etch-step,  $k + 1$ . The mismatch is illustrated in Fig. 2a.

We compensate the mismatch by introducing time compensation to the model. The time balance of the etch-step  $k$  will be compensated in step  $k + 1$  for the etching of the next cell (Fig. 2b). Thus the time of a specific etch-step  $k$ ,  $T_k$ , is not always equal to  $T$ ; rather, based on the thickness of the cell in step  $k$  ( $M_k$ ), the compensation can be computed by the following equations:

$$Tb_0 = 0, \quad M_0 = 0 \quad (4)$$

If  $M_k \geq E_s(T + Tb_{k-1})$ , then

$$T_k = T + Tb_{k-1} \quad (5)$$

$$M_{k+1} = M_k - E_s T_k \quad (6)$$

$$Tb_k = 0 \quad (7)$$

otherwise,

$$T_k = \frac{M_k}{E_s} \quad (8)$$

$$M_{k+1} = 0 \quad (9)$$

$$Tb_k = T - T_k. \quad (10)$$

The introduction of time compensation results in  $E'_s = M_k/T_k = E_s$  for any etch-step  $k$ . If the current active cell is to be removed in an etch-step  $k$ , Eq. 10 will be used to compute the time compensation; otherwise, time compensation is zero and Eq. 6 will be used to determine the resultant mass of the cell.

Wafer Orientation								
3D Lattice and top surface								
Lattice top view								
Initial virtual surface								
	3D view	Top view	3D view	Top view	3D view	Top view	3D view	Top view
Link-set type I								
Link-set type II								

Figure 3 : Top views of models in different orientations. Black and white spheres represent atoms with different link-set types.

### 3 Dynamic CA algorithm

One potential disadvantage of CA-based program lies in the fact that the program must process the entire array of crystal atoms, or cells, in parallel. Programs based on the static CA algorithm therefore require more memory to store information about cells, even idle ones (e.g. those lying in the interior of a semiconductor bulk). To significantly decrease the memory requirement and increase the speed, we have developed a dynamic method. Only atoms that are located at the interface of the silicon and the etchant are processed in relevant etch steps. These atoms exist in memory as a dynamic atom set, or a virtual surface, which contains active atoms that evolves from a masked plane to a final 3D shape. Idle cells are not processed. If an active atom is removed from the virtual surface during a given step, the neighbors will become new active atoms and be inserted into the virtual surface. The status of an active atom must be determined even though the neighbors of this active atom do not exist within the virtual surface, or have been removed in previous steps. (Each atom may have four neighbors and four links to its neighbors.) We save neighbor information to the pre-allocated space for the four links of each atom. The information is not gathered passively by the atom itself, but changed actively by its neighbors.

We have established new rules for predicting the evolution of virtual surfaces and identifying the position of newly inserted active atoms. The spatial coordinates of atoms are based on the lattice structure of silicon. For the diamond crystal lattice of silicon (Fig. 1), relevant properties of the lattice are as fol-

lows. First, there are two and only two types of atoms with different link-set types. Second, atoms with different link-set types (color coded as black or white in subsequent diagrams) are interconnected. All the neighbors of an atom with link-set type I are in link-set type II, or vice versa. Based on these properties, rules for the evolution of virtual surfaces have been developed for the first time. Three rules, E1 through E3, are summarized as follows:

- E1 A virtual surface is started in a horizontal plane. Active atoms' locations and link-set types are set based on the orientation of the lattice.
- E2 When an active atom named A1 is going to be etched away based on CA rules, its neighbors will be added to the virtual surface if they are not in the surface. The neighbors' positions are calculated from A1's position and A1's link-set types.
- E3 In the virtual surface, a newly added active atom's link-set type is the opposite of that of its neighbors.

Rules E1 and E2 are both related to the lattice's orientation, including its top-surface orientation and edge alignment. We have developed models for different orientations (Fig. 3), including wafers with surface orientation {100}, {110} or {111}.

The dynamic CA methods enables high efficiency and speed, allowing the simulation program to be run effectively on common personal computers instead of dedicated workstations. A etch simulation with a 300x300 mask could proceed at the

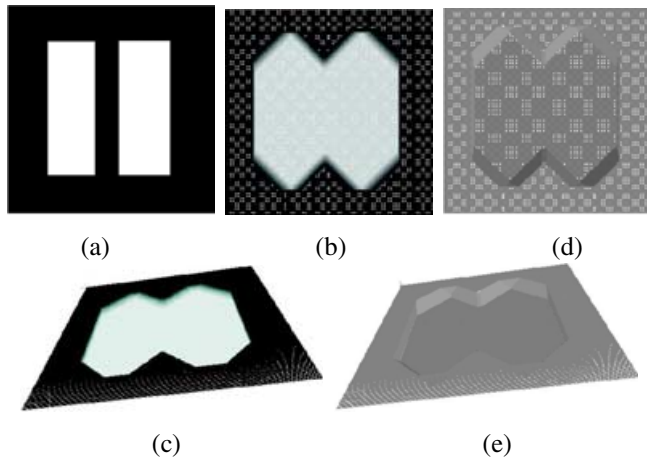


**Figure 4** : Comparison of rendering techniques: (a) mask, (b) depth-dependent rendering top view, (c) depth-dependent rendering 3D view, (d) surface-normal-dependent rendering top view, and (e) surface-normal-dependent rendering 3D view.

speed of one second per simulation step on a Pentium Pro 200 CPU. The memory requirement is significantly reduced. For instance, the requirement of memory under the dynamic method is merely 2 MB memory for a  $200 \times 200 \times 120$  lattice while the requirement under the static CA method is approximately 10 MB.

#### 4 Program implementation

Using the continuous CA model and the dynamic method, we have developed the first PC-based 3D etch simulator, named Anisotropic Crystalline Etch Simulation (ACES). The program can simulate silicon etching with different front-surface orientations in various etchants, which exhibit different etch-rate ratios. It can receive 2D mask designs in common graphic formats (including CIF, GDSII, GIF, and BMP), generate 3D profiles in standard solid-modeling formats, and display results in integrated viewers based on OpenGL or VRML.

##### 4.1 Visualization

Visualization of etching result is realized by assigning specific colors to atoms depending on specific depth within the 3D structure or by the orientation of the surfaces in which the atoms are located. For this purpose, we have set up the table for mapping the atom link status to the exact surface normal of the atom for different wafer orientations (see Tab. 2). Visualization results using two different rendering techniques are shown in Fig. 4.

##### 4.2 Surface reconstruction and edge identification

For post processes, such as finite element analysis, triangular meshes of etched 3D geometry are needed. The process to

**Table 2** : The mapping table from atom link status to surface normal.

	Neighbor				Surface Normal
	Link 1	Link 2	Link 3	Link 4	
[ 1 0 0 ]	Etchant	Etchant	Atom	Atom	(0, 0, -1)
	A	A	E	E	(0, 0, 1)
	A	E	A	E	(1, 0, 0)
	E	A	E	A	(-1, 0, 0)
	A	E	E	A	(0, 1, 0)
	E	A	A	E	(0, -1, 0)
[ 1 1 0 ]	A	E	F	F	(1, 1, 0)
	E	A	F	F	(-1, -1, 0)
	F	F	E	A	(-1, 1, 0)
	F	F	A	E	(1, -1, 0)
	F	E	A	F	(1, 0, -1)
	F	A	E	F	(-1, 0, 1)
	E	F	F	A	(-1, 0, -1)
	A	F	F	E	(1, 0, 1)
	F	E	F	A	(0, 1, -1)
	F	A	F	E	(0, -1, 1)
	E	F	A	F	(0, -1, -1)
	A	F	E	F	(0, 1, 1)
[ 1 1 1 ]	A	E	A	A	(1, 1, -1)
	E	A	E	E	(-1, -1, 1)
	E	A	A	A	(-1, -1, -1)
	A	E	E	E	(1, 1, 1)
	A	A	E	A	(-1, 1, 1)
	E	E	A	E	(1, -1, -1)
	A	A	A	E	(1, -1, 1)
	E	E	E	A	(-1, 1, -1)
[ 3 1 1 ]	A	E	F	A	(1, 3, -1)
	A	E	A	F	(3, 1, -1)
	F	E	A	A	(1, 1, -3)
	E	A	F	E	(-1, -3, 1)
	E	A	E	F	(-3, -1, 1)
	F	A	E	E	(-1, -1, 3)
	E	A	F	A	(-3, -1, -1)
	E	A	A	F	(-1, -3, -1)
	E	F	A	A	(-1, -1, -3)
	A	E	E	F	(3, 1, 1)
	A	E	F	E	(1, 3, 1)
	A	F	E	E	(1, 1, 3)
F	A	E	A	(-3, 1, 1)	



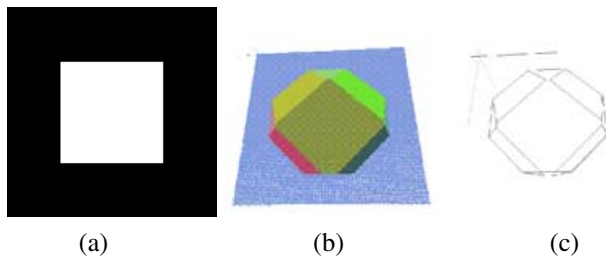


**Figure 5** : An example of the edge detection method: (a) mask shape, (b) 3D view of the simulation result in atom model, and (c) 3D view of the simulation result in edge model.

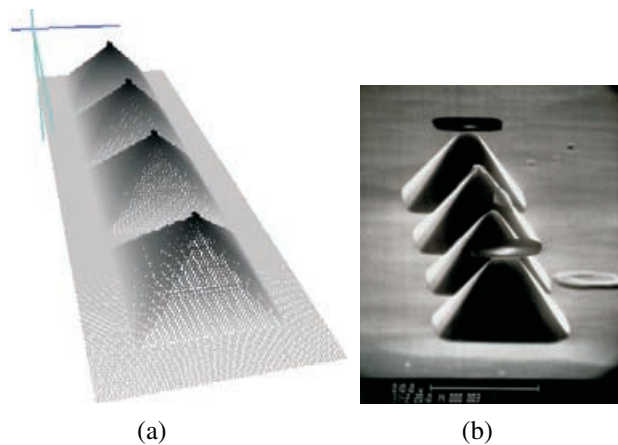


**Figure 6** : Comparison of simulation and experimental results for an anisotropically etched tip array: (a) simulation result and (b) experimental result.

convert a simulation result from a set of atoms to a triangular mesh is called surface reconstruction. A number of methods are available in the computer graphics literature [Galand and Heckbert (1995), Garland and Heckbert (1997), Heckbert and Garland (1997), Hoppe, DeRose, Duchamp, McDonald and Stuetzle (1993)], but none of them is well fitted for this case. We have developed an edge detection method to perform the conversion efficiently although there might be problems with small features. The method consists of three steps:

1. Plane identification. For all atoms in the entire virtual surface  $V_N$ , and scanning  $V_N$  in a fixed order:

Locate the next unallocated atom,  $V_N(i, j)$ , such that it has more than three neighbors in the same orientation.

Based on the atom's position and orientation, generate a new polygon object  $P(k)$  and compute its plane equation.

Starting from  $V_N(i, j)$ , expand and mark atoms that have the same orientation and also fit the plane equation. Save all visited atoms in  $P(k)$ .

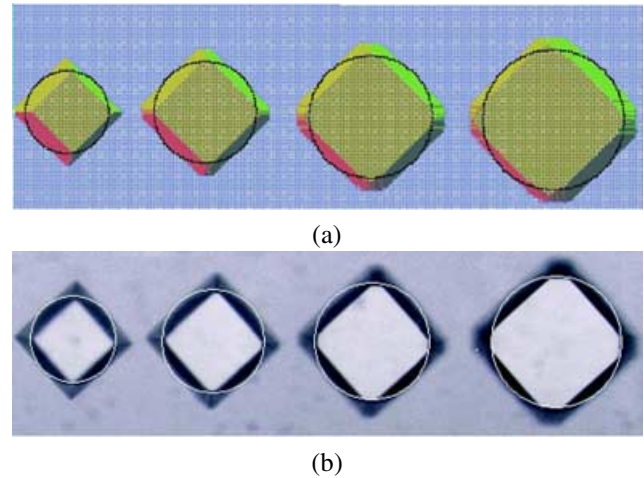


**Figure 7** : Comparison of simulation and etching results using a set of circles in different diameters: (a) simulation and (b) experimental. The dark circles in (a) and light circles in (b) represent original mask shapes.

2. Neighbor identification. For all polygons generated in step 1:

For all atoms in polygon  $P(k)$ , find its neighbor atom that belongs to another polygon  $P(k1)$ , mark  $P(k)$  and  $P(k1)$  as neighbor.

3. Edge computation. For all polygons:

Locate the next polygon  $P(k)$  that intersect with three other polygons  $P(k1)$ ,  $P(k2)$  and  $P(k3)$ . Generate a new edge object  $E(m)$  and compute one end point of  $E(m)$  from the intersection of  $P(k)$ ,  $P(k1)$  and  $P(k2)$ . Compute the other end point of  $E(m)$  from the intersection of  $P(k)$ ,  $P(k2)$  and  $P(k3)$ .

The edge detection method works especially well when the virtual surface of a simulation result mainly contains all the major planes in silicon lattice. Fig. 3 shows an example of edge detection.

## 5 Etch tests and program validation

### 5.1 Three-dimensional shape verification

We have applied the simulation program to anisotropic silicon tips using a square mask with the edges aligned in the  $\langle 100 \rangle$  direction. The tip is formed by etching  $\langle 100 \rangle$ -oriented surfaces vertically using EDP or KOH solutions. The simulation results (Fig. 6a), obtained by using the continuous CA model with an etch-rate ratio of  $\{100\}:\{110\}:\{111\} = 1:0.13:0$ , is well matched with the experimental result (Fig. 6b). A second test pattern contains open circles with different diameters. The matched simulation and experimental results are shown in Fig. 7.

## 5.2 Etch rate diagram verification

First, we simulated the etching of a spoke pattern, which is a commonly used feature to visualize the etch-rate distribution. Fig. 8a is a simulation result of spoke pattern etching. It matches well with the experimental result, shown in Fig. 8b. However, this method does not yield precise etch rates because the resolution of the physical mask is limited.

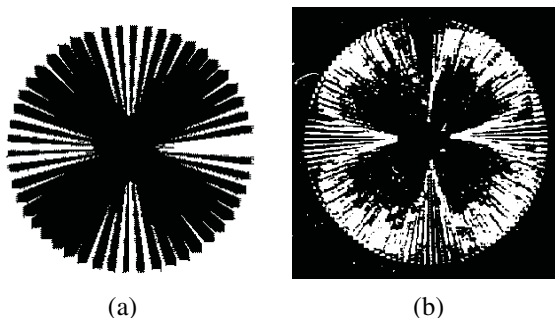


**Figure 8** : Comparison of simulation and etching results using a spoke pattern: (a) simulation result and (b) experimental result.

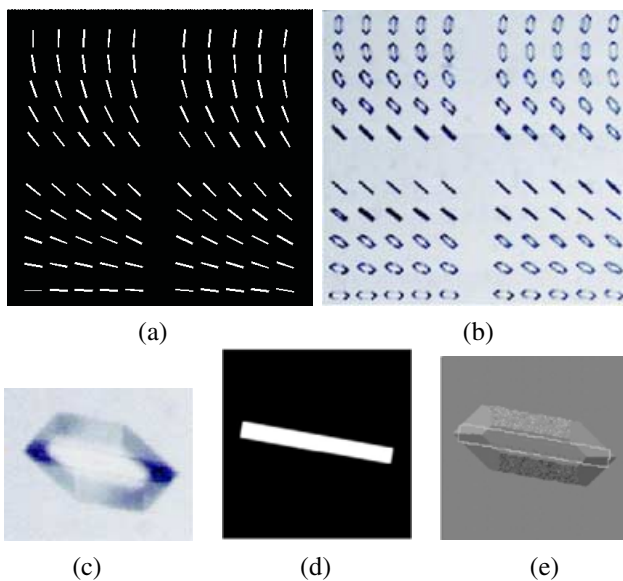


**Figure 9** : The etching experiment and simulation for EDP etch rate diagram: (a) mask containing rotating rectangles with 1 angle interval, (b) etching result of the whole pattern in EDP solution, (c) etching result of a single rotated rectangle in EDP solution, (d) rotated rectangle mask for etching simulation, and (e) simulation result.

We have developed a new methodology for obtaining the etch rate diagram with high angular resolution. To our knowledge,

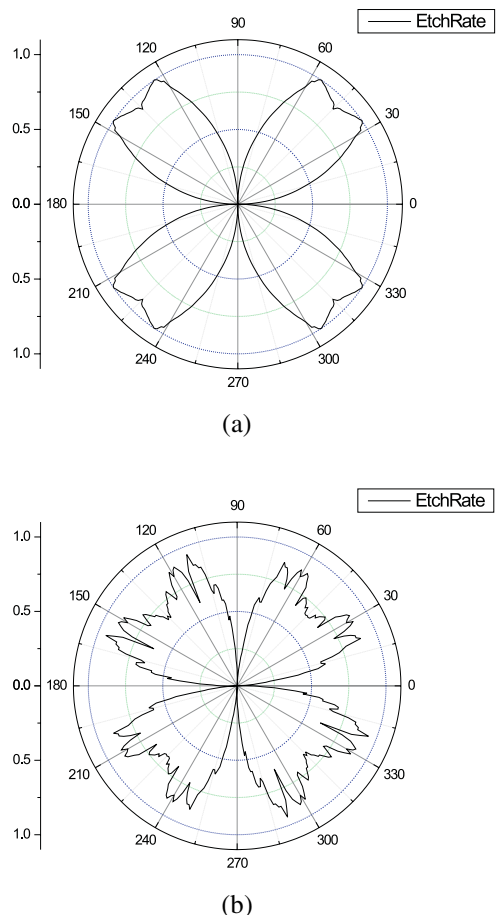


**Figure 10** : Calibrated etch-rate diagram when the substrate front surface is  $\{100\}$ : (a) etch-rate diagram from simulation, and (b) etch-rate diagram from experiment with etchant EDP.

such a method has not been demonstrated in the past. A set of rectangular holes, each being  $80\text{-}\mu\text{m}$ -long and  $10\text{-}\mu\text{m}$ -wide, with  $1^\circ$  increments in angular positions, is designed (Fig. 9a). Etching for a relatively short period of time, the profile of the undercut cavity is parallel with the long edge of the rectangle. Therefore, the etch rate associated with a particular orientation can be obtained by measuring the amount of lateral undercuts along the long edges. Since the entire lattice is used to achieve a single etch rate, many more simulation steps could be applied to the lattice to obtain measurable amount of undercut, and relatively precise etch rates would result compared with the spoke-pattern etching.

The etch rate diagram for  $\{100\}$  silicon orientation (Fig. 10a) is shown as example. The experimental result (Fig. 10b) is matched with the simulation result although difference in details still exist because high-index planes are not implemented in this CA model. A single rectangle (Fig. 10c-e) has been

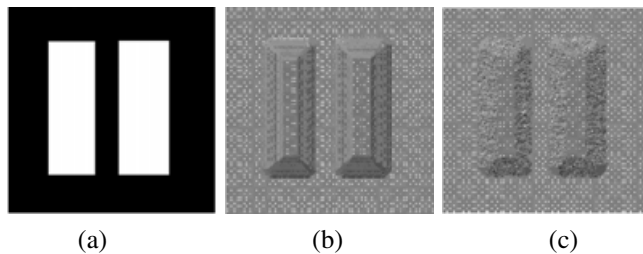


**Figure 11** : Different simulation results with the continuous CA model and the stochastic CA model: (a) mask, (b) etch results (top view) generated by continuous CA model, and (c) results by stochastic CA model. Sidewalls are much more smooth in (b).

magnified to show the match of the 3D shapes.

### 5.3 Stochastic CA model versus continuous

Etch results obtained using a stochastic CA model and a continuous CA model are presented in Fig. 11 to illustrate the different results. The simulation results of a double rectangle mask (Fig. 11a) with these two models, with designated etch rate ratios of  $\{100\}:\{110\}:\{311\}:\{111\} = 1:0.5:0.5:0.05$ , are shown in Fig. 11b and 11c. The resulting  $\{111\}$  planes based on the continuous CA model are much smoother compared with that based on the stochastic CA model.

## 6 Conclusions

Anisotropic etching of silicon is a key technique for realizing 3D MEMS structures. As MEMS design and fabrication become increasingly sophisticated, efficient and accurate anisotropic etching simulation becomes more important. We present an Anisotropic Crystalline Etching Simulation (ACES) program based on a novel continuous cellular automata (CA) model and a dynamic method. The continuous CA model greatly extended the capability of CA model, enabling high accuracy and high efficiency of simulation. The dynamic CA technique resulted in increased simulation speed and reduced memory requirements. Experiments have validated the continuous CA model and the dynamic method. A new method for obtaining the etch rate diagram has been demonstrated.

**Acknowledgement:** This work is supported by the DARPA Composite CAD program under contract F30602-97-2-0328.

## References

**Asaumi, K.; Iriye, Y.; Sato, K.** (1997): Anisotropic-etching process simulation system MICROCAD analyzing complete 3D etching profiles of single crystal silicon. *Tenth Annual International Workshop on Micro Electro Mechanical Systems of IEEE*, pp. 412–417.

**Bean, K. E.** (1978): Anisotropic etching of silicon. *IEEE Transactions on ED*, vol. 25, pp. 1178–1185.

**Buser, R. A.; de Rooij, N. F.** (1991): ASEP: A CAD program for Si anisotropic etching. *Sensors and Actuators*, vol. 28, pp. 71–78.

**Buttgenbach, S.; Than, O.** (1996): SUZANA: A 3D CAD tool for anisotropically etched silicon microstructures. In *Proceedings of European Design and Test Conference ED&TC 96*, pp. 454–458, IEEE Computational Soc. Press.

**Danel, J. S.; Delapierre, G.** (1992): Anisotropic crystal etching: A simulation program. *Sensors and Actuators*, vol. 31, pp. 267–274.

**Frank, F. C.; Ives, M. B.** (1960): Orientation dependent dissolution of Ge. *Journal of Applied Physics*, vol. 31, pp. 1996–1999.

**Garland, M.; Heckbert, P. S.** (1995): *Fast polygonal approximation of terrains and height fields*. Tech. Rep. CMU-CS-95-18.

**Garland, M.; Heckbert, P. S.** (1997): Surface simplification using quadric error metrics. In *Computer Graphics Proceedings of SIGGRAPH 97*, pp. 209–216, New York NY.

**Heckbert, P. S.; Garland, M.** (1997): Survey of polygonal surface simplification algorithms. In *Computer Graphics Proceedings of SIGGRAPH 97*. New York NY.

**Heim, U.** (1993): A new approach for the determination of the shape of etched devices. *Journal of MEMS*, vol. 3, pp. 116–117.

**Hoppe, H.; DeRose, T.; Duchamp, T.; McDonald, J.; Stuetzle, W.** (1993): Mesh optimization. In *Computer Graphics Proceeding*, pp. 19–26, New York NY.

**Hubbard, T. J.; Antonsson, E. K.** (1994): Emerging faces in crystal etching. *Journal of MEMS*, vol. 3, pp. 19–28.

**Jaccodine, R.** (1962): Use of modified free energy theorems to predict equilibrium growing and etching shapes. *Journal of Applied Physics*, vol. 33, pp. 2643–2647.

**Karam, J. M.; Courtois, B.** (1996): From the MEMS idea to the MEMS product: CAD and foundries. In *Wescon/96 Conference Proceedings*, pp. 73–78, New York NY.

**Li, G.; Hubbard, T.; Antonsson, E. K.** (1998): SEGS: On-line www web etch simulator. In *IEEE MSM 98*, Santa Clara CA.

**Ling, C. G.; Rebeiz, G. M.** (1992): 94 GHz integrated horn monopulse antennas. *IEEE Transactions on Antennas & Propagation*, vol. 40, pp. 981–984.



**Liu, C.; Gamble, R.** (1998): Mass producible monolithic silicon probes for scanning probe microscopes. *Sensors and Actuators A Physical*, vol. 71, no. 3, pp. 233–237.

**Madou, M.** (1997): *Fundamentals of Microfabrication*. CRC Press, Boca Raton, FL.

**Marchetti, J.; He, Y.; Than, O.; Akkaraju, S.** (1998): Efficient process development for bulk silicon etching using cellular automata simulation techniques. In *SPIE Conference on Micromachined Devices and Components IV*, pp. 287–295, Santa Clara CA.

**Nishidate, K.; Baba, M.; Gaylord, R.** (1998): ASECA: A cellular-automata simulation program for a silicon anisotropic super-micro-etching process in aqueous KOH. *Computers in Physics*, vol. 12, pp. 88–93.

**Petersen, K. E.** (1982): Silicon as a mechanical material. *Proceedings of IEEE*, vol. 70, pp. 420–457.

**Senturia, S.; Aluru, N.; White, J.** (1997): Simulating the behavior of MEMS devices: Computational methods and needs. *IEEE Computational Sci. and Engr*, vol. 4, pp. 30–43.

**Sequin, C. H.** (1991): Computer simulation of anisotropic crystal etching. In *Transducers 91*, pp. 801–806, Chicago, IL.

**Shaw, D. W.** (1979): Morphology analysis in localized crystal growth and dissolution. *Journal of Crystal Growth*, vol. 47, pp. 509–517.

**Than, O.; Buttgenbach, S.** (1994): Simulation of anisotropic chemical etching of crystalline silicon using a cellular automata model. *Sensors and Actuators A*, vol. 45, pp. 85–88.

**Wright, J. A.; Tatic-Lucic, S.; Tai, Y. C.; Maher, M. P.; Dvorak, H.; Pine, J.** (1996): Towards a functional MEMS neurowell by physiological experimentation. In *Proceedings of the 1996 International Mechanical Engineering Congress and Exposition*, pp. 333–338, Atlanta GA.

